Elevating mechanical performance of cementitious composites with surface-modified 3D-Printed polymeric reinforcements

Xu, Yading; Wan, Zhi; Šavija, Branko

DOI
10.1016/j.dibe.2024.100522

Publication date
2024

Document Version
Final published version

Published in
Developments in the Built Environment

Citation (APA)
Xu, Y., Wan, Z., & Šavija, B. (2024). Elevating mechanical performance of cementitious composites with surface-modified 3D-Printed polymeric reinforcements. *Developments in the Built Environment*, *19*, Article 100522. https://doi.org/10.1016/j.dibe.2024.100522

Developments in the Built Environment 19 (2024) 100522

Contents lists available at ScienceDirect

Developments in the Built Environment

journal homepage: www.sciencedirect.com/journal/developments-in-the-built-environment

Elevating mechanical performance of cementitious composites with surface-modified 3D-Printed polymeric reinforcements

Yading Xu [a], Zhi Wan [b], Branko Šavija [a,*]

[a] Microlab, Delft University of Technology, the Netherlands
[b] Department of Civil and Environmental Engineering, University of California, Los Angeles, USA

ARTICLE INFO

Keywords:
3D printed reinforcement
Strain-hardening cementitious composites
Surface modification

ABSTRACT

3D printed polymeric reinforcement has been found able to improve the ductility of cementitious materials. However, due to the hydrophobic nature of commonly used 3D printing polymers, the bonding strength between the 3D printed polymers and cementitious matrix is extremely weak, which potentially hinders the mechanical performance of the reinforced composites. This work aims to improve the bonding properties by applying surface modifications on the 3D printed reinforcement, and eventually enhance the mechanical performance of the reinforced cementitious composites. Three types of surface coatings ingredients: epoxy resin (EP), sand sprinkled epoxy (SA) and short steel fibers sprinkled epoxy (SF) were used. Pull-out experiments are performed to study the bonding properties of the 3D printed reinforcement with different coatings. Then, uniaxial tensile and four-point-bending experiments are used to investigate the mechanical performance of the reinforced cementitious composites. A lattice type numerical model is applied to simulate the pull-out and tensile tests. The pull-out experiments indicate that the SA and SF reinforcement achieved approximately two times higher bonding strength than the uncoated and EP reinforcement. The tensile and flexural results suggest that the cementitious composites with SA and SF reinforcement achieved significantly better ductility (manifested by strain-hardening and deflection-hardening behavior) than the composites with uncoated and EP reinforcement. The numerical simulation results highly agree with the experimental findings, and further confirmed that the improved reinforcement-mortar bonding strength is the determinative factor that enhanced the composites mechanical performance. The findings of this work suggest that the sand and steel fiber surface coatings can effectively enhance the ductility of cementitious composites reinforced by 3D printed polymers.

1. Introduction

Concrete is one of the most widely used engineering materials. Due to the intrinsic brittleness, especially under tensile load, concrete is often reinforced by other materials to ensure the mechanical performance. Conventional reinforcement materials, such as steel rebars, fibers (Zhou et al., 2021) and textiles (Rafique et al., 2020; Valeri et al., 2020a) are frequently used in engineering applications. When integrated with concrete, these reinforcements can take over the load after a crack appears, and prevent the crack from further propagation.

Traditionally, these reinforcement materials either need to be manually placed in position, or added to concrete mixtures during mixing. In recent years, a trend of digitalization has emerged in the civil engineering field. Using 3D printing technology to fabricate reinforcement for concrete and other cementitious materials has started to attract more and more research attention. A typical example is in-process inserting of a steel cable while extruding concrete/geopolymers as reported by (Lim et al., 2018; Li et al., 2020a). This technique allows the reinforcement to be embedded in each printed concrete layers, allowing the printed concrete with anisotropic ductility dominated by the printing configuration. In addition, fibers (Liu et al., 2023; Chaves Figueiredo et al., 2019) were also used as reinforcement in the context of direct 3D concrete printing. The feasibility of using 3D printed (arch welding) steel rebar as reinforcement was also studied by (Mechtcherine et al., 2018), and it was found that the printed rebars have slightly lower strength and weaker bond with concrete than conventional rebars. Compared to printing steel, there are significantly more studies focusing on using polymeric materials to print reinforcement for cementitious materials.

Owing to the rapid development of desktop 3D printers, polymeric

* Corresponding author.
E-mail address: b.savija@tudelft.nl (B. Šavija).

https://doi.org/10.1016/j.dibe.2024.100522
Received 29 May 2024; Received in revised form 26 July 2024; Accepted 9 August 2024
Available online 15 August 2024

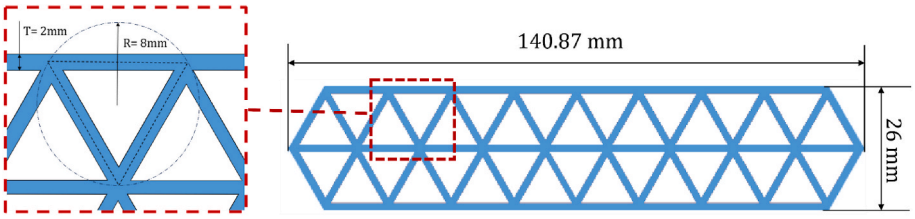

Fig. 1. Design parameters of the reinforcement structures.

Table 1
Printing parameters.

Parameters	Configuration
Nozzle diameter (mm)	0.8
Temperature (°C)	260
Layer height (mm)	0.2
Line width (mm)	0.7
Infill density (%)	100
Printing speed (mm/s)	40

Table 2
Reinforcement surface treatment methods.

Specimen	Surface coating
ABS	None
EP	Epoxy
SA	Epoxy and sand
SF	Epoxy and steel fiber

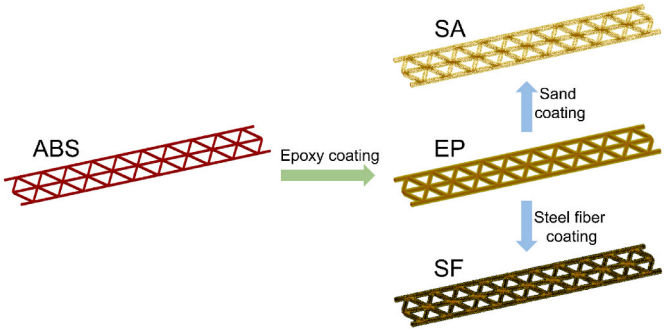

Fig. 2. Schematics of ABS reinforcement surface modification.

reinforcement with complex structures can be fabricated and used as reinforcement. In our previous study (Xu et al., 2019), it was found that cementitious mortar reinforced by 3D printed planar lattice structures achieved the so-called "strain-hardening" behavior (Li et al., 2020b; Zhu et al., 2024; Lao et al., 2024), although it requires relatively higher reinforcing ratio than traditional steel reinforcement. Similar results were also found in other studies with spatial three-dimensional structure (Salazar et al., 2020). One advantage of 3D printing technology is the high customizability, which allows fabricating reinforcement that difficult to obtain by traditional techniques, for instance reinforcement with optimized geometry according to the actual loading condition. Previously, with the aid of 3D printing techniques, it was found that the mechanical properties of cementitious lattice structure could be optimized by tailoring the lattice designs (Dey et al., 2023; Xu et al., 2022). In terms of the reinforcement, functionally graded designs (Xu et al., 2019, 2021; Tang et al., 2023) of polymeric lattice structure reinforcement have also been found able to improve flexural resistance of cementitious beams while reducing reinforcing ratio. Apart from lattice structures, 3D printed minimal surface gyroid structures (Skoratko et al., 2022; Nguyen-Van et al., 2022a, 2022b) were also used as reinforcement and they were found able to improve ductility of cementitious beams. Not only the improvement in tension/flexural properties, 3D printed polymeric structures were also found able to improve compressive performance of conventional cementitious materials. This was achieved by taking advantage a special type of structures with auxetic behavior (negative Poisson's ratio) (Chen et al., 2023; Xu et al., 2024a, 2024b). Under compression, these auxetic structures exhibit lateral contraction which limits crack propagation in the cementitious materials thus enhancing the ductility.

For conventional reinforcement, it is well known that the bond properties between the reinforcement and cementitious matrix have critical impact on the mechanical performance of the reinforced composites (Li et al., 2024; Reis et al., 2023; Sigrüner et al., 2023). For example, steel rebars are often ribbed to increase the physical interlocking effect (Reis et al., 2023; Ertzibengoa et al., 2012; Rabi et al., 2020; Abbas et al., 2023) and achieve good bond with the cementitious

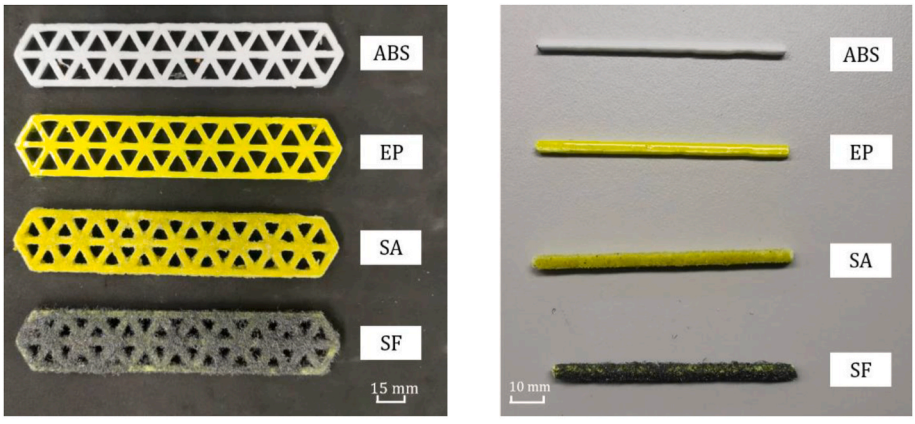

Fig. 3. Printed and surface-modified a) lattice reinforcements, b) bars for pull-out test.

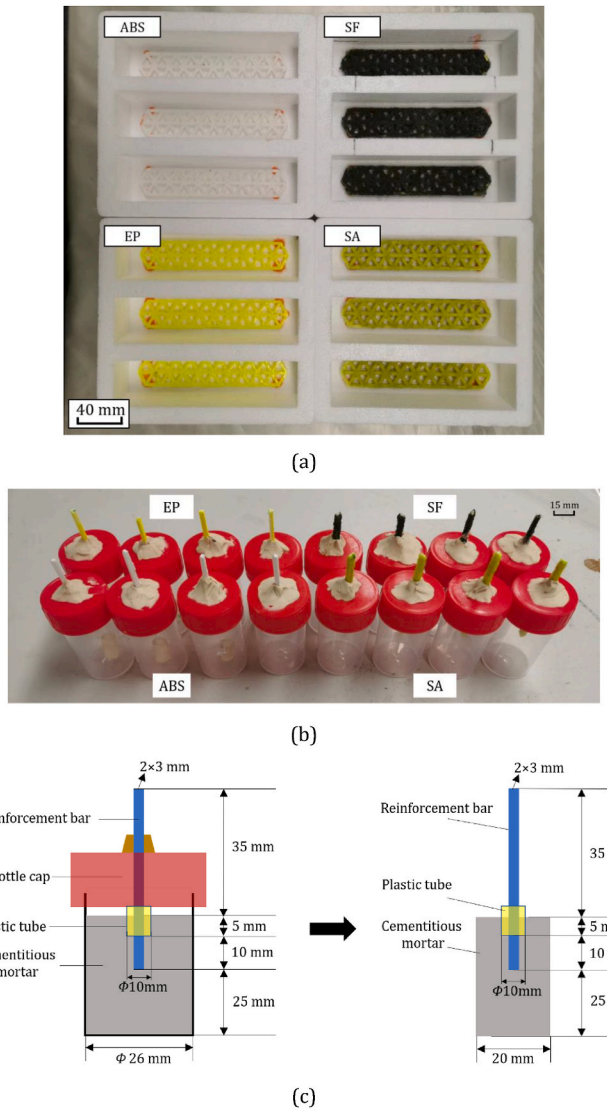

Fig. 4. a) Reinforcement glued in Styrofoam molds, b) bars fixed in cylindrical molds, c) dimensions of the pull-out specimens.

Table 3
Mixture design of the matrix material (g/l).

CEM I 42.5 N	Fly ash	Sand (0.125–0.250 mm)	Superplasticizer (Glenium 51)	Water
550	650	550	2	395

matrix. In terms of polymeric reinforcement, such as textiles, coating techniques are often used to increase the bond properties with the cementitious matrix. For instance, sand coating was found to improve the interlocking between polymeric reinforcement (Preinstorfer et al., 2023; Lu et al., 2021; Cho et al., 2006) and concrete, as the sand particles significantly increase the surface roughness of the reinforcement. Hydrophilic materials (Alatawna et al., 2021; Halvaei et al., 2018) were also used as surface coating to increase the adhesion between the polymeric reinforcement and the cementitious matrix. As for the 3D printed polymeric reinforcement, it was already noticed in several studies (Nguyen-Van et al., 2022a; Xu et al., 2024a, 2024b) that the printed reinforcement has rather weak bonding with cementitious matrix. A few preliminary studies (Xu et al., 2019; Farina et al., 2016) have shown that directly printing rough texture on the reinforcement surface

Fig. 5. Demolded specimens.

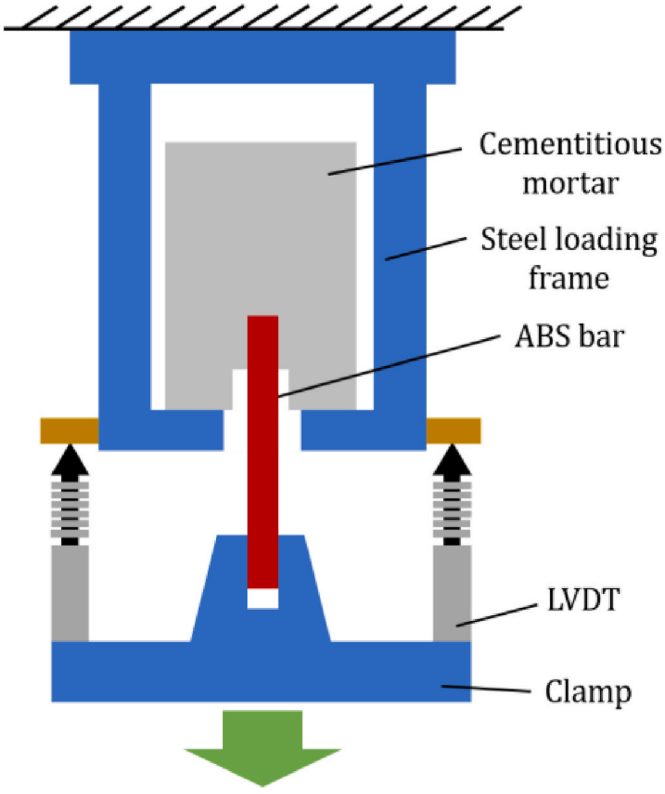

Fig. 6. Schematics of the pull-out test set-up.

would give the reinforced cementitious composites improved mechanical properties. However, the potential of using surface coating on 3D printed polymeric reinforcement to improve the mechanical performance of the reinforced composites has not been investigated yet.

This work focuses on using surface modification approaches to improve mechanical properties of cementitious composites reinforced by 3D printed polymeric reinforcement. Four types of surface coatings are introduced to the 3D printed reinforcement. Pull-out tests are performed to evaluate the interface bond behavior between the reinforcement and cementitious mortar. Flexural and uniaxial tensile testes are performed to study the mechanical performance of the reinforced cementitious composites. In addition to experiment, numerical

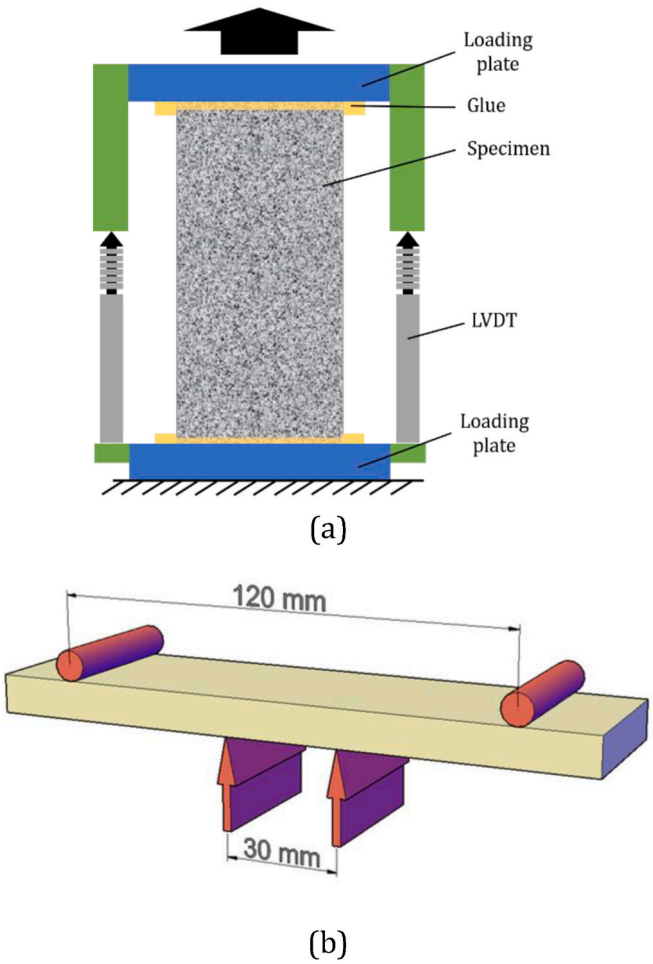

Fig. 7. Schematics of the experimental set-up for a) uniaxial tension and b) four-point-bending.

modeling is also adopted to help better understand and analyze the experimental results. A lattice type numerical model (Xu et al., 2019, 2022; Schlangen et al., 1997) is adopted to simulate the mechanical experiment. Based on the obtained results, the critical role of different surface coatings on determining the pull-out behavior and the fracture behavior of the reinforced cementitious composites is given in the present work.

2. Methods and materials

2.1. Specimen preparation

2.1.1. Design and printing of the reinforcement

In order to provide fair comparisons, the design and printing process of the lattice reinforcement design is kept constant as the large triangle design reported in our previous study (Xu et al., 2019). The design parameters can be found in Fig. 1. To ensure the reinforcement placed in the middle of the specimen, stands on the corner were also designed, such that the reinforcement can be glued in the molds to the designed position. A commercial FDM (fused deposition modeling) 3D printer Ultmaker 2+ was used to print the designed meshes, using ABS (Acrylonitrile Butadiene Styrene) as printing material. The printing parameters are listed in Table 1. The tensile strength of the printed ABS is 34.3 MPa, and the elongation ratio at break is 3.1 %. In the meanwhile, to investigate the interface bonding properties between the printed reinforcement and the cementitious mortar, ABS bars were also printed following the same printing parameters. Later, the ABS bars were casted in cementitious mortar and used for pull-out tests.

2.1.2. Surface treatment of the printed reinforcement

Three types of surface treatment methods were applied on the printed ABS reinforcements and ABS bars: epoxy coating; epoxy and sand coating; epoxy and steel fiber coating (see Table 2). The surface treatment procedures are as follows (schematics of the surface modification is shown in Fig. 2):

- A two-component epoxy was mixed (100 g Conpox Resin BY 158 and 30 g Conpox Hardener BY 2996).
- The ABS reinforcement and ABS bars were submerged in the epoxy mixture for 10 min.
- The specimen was evenly divided into three batches: EP, SA and ST. The EP batch was stored in room temperature for 24 h; The SA batch was thoroughly submerged in a box with fine sand (0.125–0.250 μm), and vibrated for 1 min, afterwards transferred to a flat surface and stored for 24 h; The SF was modified following the same procedure as the SA, however, using a short steel fiber bath.

In total, four types of reinforcement, and bar samples were prepared as shown in Fig. 3. All the reinforcements were glued on the stands in Styrofoam molds using silicon rubber (see Fig. 4a), preparing for uniaxial tensile and four-point-bending tests. All bar samples were fixed on plastic cylindrical bottle molds (see Fig. 4b), preparing for pull-out tests. Cementitious mortar was casted inside the bottle. After curing,

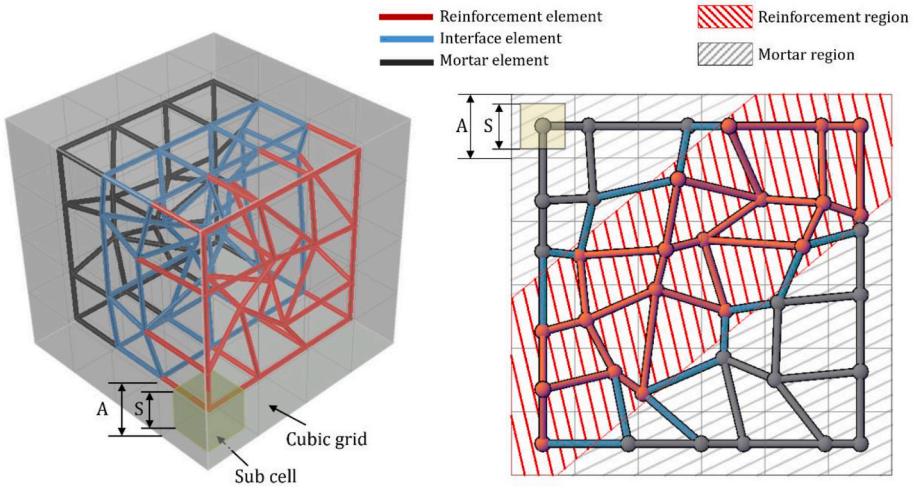

Fig. 8. Schematics of the lattice network generation, 3D (left) and 2D (right) views are shown.

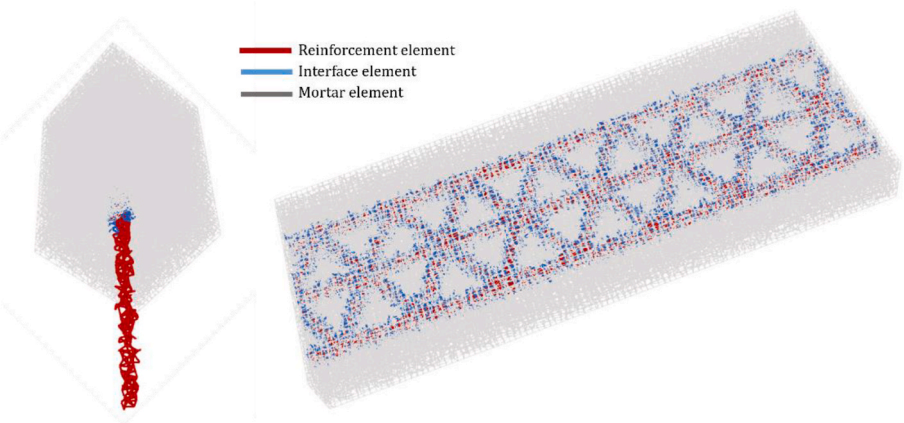

Fig. 9. Generated lattice network for the pull-out test (left) and tensile test (right).

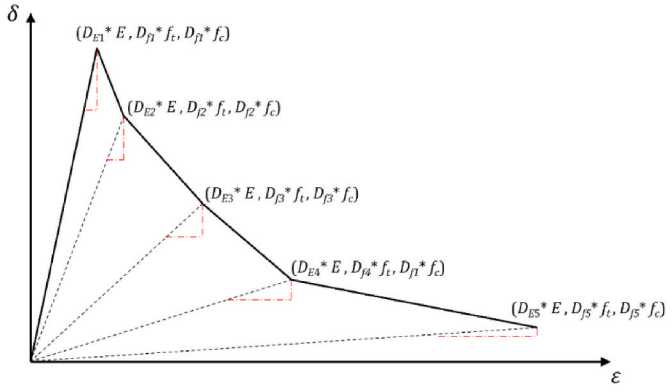

Fig. 10. Schematics of the input behavior with multiple linear segments.

cylindrical specimens were demolded from the bottles and cut into designed dimensions for the pull-out tests. The dimensions of the pull-out specimens are shown in Fig. 4c.

2.1.3. Mixing, casting and curing

Three series of specimens were casted: pull-out test specimens, four-point-bending test specimens, and tensile test specimens. The cementitious mixture proportion was kept the same as (Xu et al., 2019), and listed in Table 3.

Weighted dry materials were first mixed for 4 min, then water and superplasticizer were added, followed by another 4 min of mixing. Subsequently, the fresh mixture was casted in the Styrofoam and cylindrical bottle molds. One day after casting, all specimens were demolded (see Fig. 5) and stored in a curing room (20 ± 2 °C, 96 ± 2% RH) until the age of 28 days. Before testing, the specimens for tensile and pull-out tests were cut to comply with corresponding test methods. The dimension of the specimens tested in tension is 100 × 40 × 10 mm, and the dimension of the test specimens in four-point-bending is 160 × 40 × 10 mm. The specimens for tensile tests were painted in white and sprayed with black dots for digital image correlation (DIC) analysis.

2.2. Experiments

2.2.1. Pull-out tests

The test set-up for the pull-out test is shown in Fig. 6. A hydraulic press INSTRON 8872 is used to perform the test. During the test, the specimen is placed inside the steel frame which is fixed on the INSTRON. A straight downwards uniaxial load is applied on the ABS bar by a clamp, at a constant rate of 0.005 mm/s. The load and displacement data are recorded by the hydraulic press and LVDTs (linear variable differential transducers), respectively.

2.2.2. Uniaxial tension and four-point bending tests

To provide fair comparison, the uniaxial and four-point-bending tests experiment set-up and the loading rate are kept the same as our previous work (Xu et al., 2019). The tests are performed by the same hydraulic press INSTRON 8872 as mentioned before. The schematics of the uniaxial tension tests are shown in Fig. 7a. The specimen is glued on the loading plates, and uniaxial load with a constant rate of 0.005 mm/s is applied on the loading plates. The load and displacement data are recorded during the test by the INSTRON 8872 load cell and LVDT (see Fig. 7a), respectively. During the tensile experiments, a digital camera is placed in front of the specimens and took pictures for DIC tests. The schematic of the four-point-bending tests are shown in Fig. 7b. The load span is 120 mm and the midspan is 30 mm. Displacement controlled upwards load was applied on the specimen by the rigid support, at a constant rate of 0.01 mm/s. The load is recorded by the load cell and the

Table 4
Input parameters of the composites under pull-out and uniaxial tensile tests by the lattice model[a].

Element Type	Material properties (MPa)			Segment 1		Segment 2		Segment 3		Segment 4		Segment 5	
	E	f_t	f_c	D_{E1}	D_{f1}	D_{E2}	D_{f2}	D_{E3}	D_{f3}	D_{E4}	D_{f4}	D_{E5}	D_{f5}
Mortar	11417	3	$-8^{a} f_t$	1	1	–							
ABS	1590	35	$-2^{a} f_t$	1	1	0.5	1	–					
EP	1590	42	$-2^{a} f_t$	1	1	0.6	1	0.3	0.7	0.1	0.6	0.02	0.6
SA	2380	43	$-2^{a} f_t$	1	1	0.6	1	0.3	0.7	0.1	0.6	0.02	0.6
SF	3694	45	$-2^{a} f_t$	1	1	0.6	1	0.3	0.7	0.1	0.6	0.02	0.6
ABS-M	150	2.2	$-f_t$	1	0.6	0.3	1	0.1	1	0.03	1	–	
EP-M	230	2.5	$-f_t$	1	0.6	0.3	1	0.1	1	0.03	1	–	
SA-M	6899	35	$-f_t$	1	0.6	0.3	1	0.1	1	0.03	1	–	
SF-M	7555	45	$-f_t$	1	1	0.6	1	–					

[a] ABS, EP, SA and SF represent the reinforcement elements; ABS-M, EP-M, SA-M, and SF-M represent the corresponding interface elements.

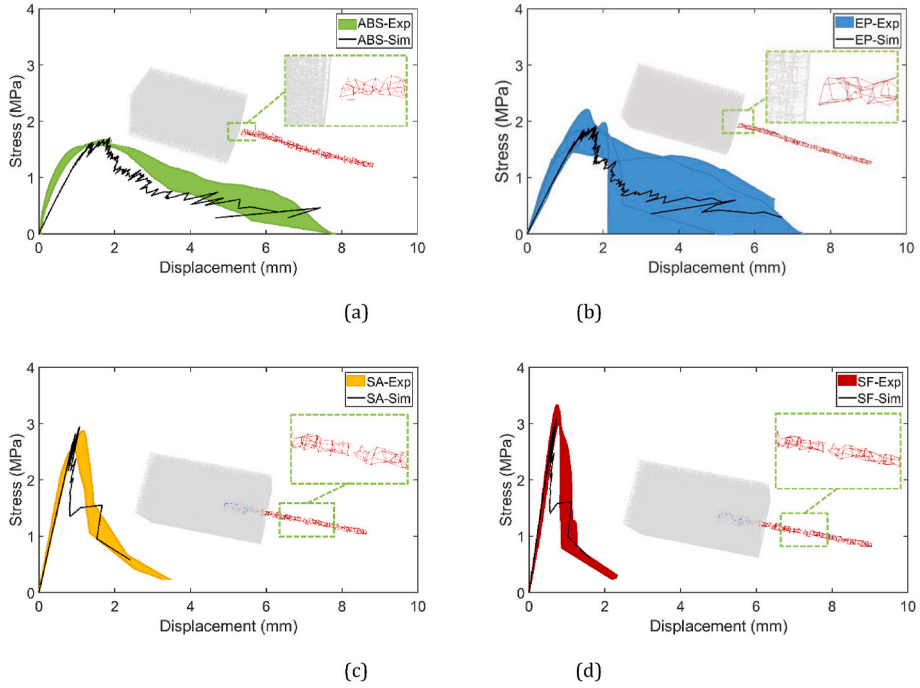

Fig. 11. Comparison of the pull-out load-displacement curves obtained from experiments and simulation, a) ABS, b) Epoxy coated, c) sand coated and d) steel fiber coated reinforcement, fracture mode of the pull-out simulation is also shown.

displacement is recorded by the LVDTs placed at the midspan of the specimen.

3. Numerical modeling

Previously, the delft Lattice model has been successfully extended to simulate the fracture of SHCCs reinforced by 3D printed meshes (Xu et al., 2019) under four-point-bending load. The numerical results showed good agreement with the experiment, however, the critical role of the reinforcement-mortar interface was not fully understood under uniaxial tension. Therefore, this work focuses on further clarifying the impact of the reinforcement-mortar interface properties on the uniaxial tensile properties of the composites, based on an experimentally validated lattice model. The general lattice modeling procedures are the same as our previous studies (Xu et al., 2019, 2022). The main difference is that, in this work, the interface properties are experimentally validated. The lattice modeling procedures are described in the following sub-sections.

3.1. Lattice network construction

The lattice network was constructed by the following procedures:

- A domain with the same dimension (100 × 40 × 10 mm) of the tensile tested composites specimens was generated using unit cubic grids (1 × 1 × 1 mm).
- One node was placed in a sub-cell (shown in Fig. 8) inside each cubic grid. The ratio between the size of the grid (A) and the sub-cell (S) was defined as the randomness (R) of the lattice network. In this work, $R = 0.99$ was used to ensure realistic crack pattern (Schlangen et al., 1997), while the nodes in the outermost surfaces of the domain were aligned such that the load can be applied evenly on the specimen.
- The node in the adjacent grids were connected to form a lattice network. Depending on the position of the nodes, three different types of elements were defined: reinforcement elements have both nodes locating in the reinforcement region, mortar elements have both nodes locating in the mortar region and the others were interface elements, as depicted in Fig. 8. The generated lattice network for the pull-out test and tensile test is shown in Fig. 9.

3.2. Calibration of model inputs

The calibration procedures for the input parameters of the cementitious mortar was maintained the same as clarified in our previous study (Xu et al., 2019). To better capture the pull-out and softening behavior, multiple linear segment constitutive behavior (as indicated in Fig. 10) was used as the reinforcement and the interface input behavior. The calibration simulations were executed using these input behaviors to fit the pull-out experiment results. The calibrated input parameters are listed in Table 4. The results of pull-out experiment and the corresponding simulation results will be presented in the.

4. Experimental results

4.1. Pull-out behavior

From the view of molecular structure, the ABS is a type of polymers without hydrophilic groups. This means that there is hardly any chemical bond between the ABS reinforcement and the cementitious matrix. Therefore, the bond strength between the untreated ABS reinforcement was expected to be weak. This can be seen from the pull-out results of the ABS in Fig. 11a, the stress-displacement curves of the untreated ABS (Fig. 11a ABS-Exp) show similar slip response of conventional straight fibers being pulled-out from concrete, as seen in many previous studies (Sigrüner et al., 2023; Wu et al., 2023). In this sense, the peak stress of the ABS pull-out curve indicates the frictional bond strength of the reinforcement-mortar interface, which is approximately 1.5 MPa. This value is considerably lower than the chemical bond strength between PVA (Polyvinyl Alcohol) fiber and cementitious mortar, while it reaches the frictional bond strength range between PVA fiber (1 MPa–3.5 MPa) (Redon et al., 2001) and cementitious mortar. After coating with epoxy, the bond strength of EP (see Fig. 11b EP-Exp) is slightly improved to approximately 2 MPa, however, still no obvious chemical bond can be

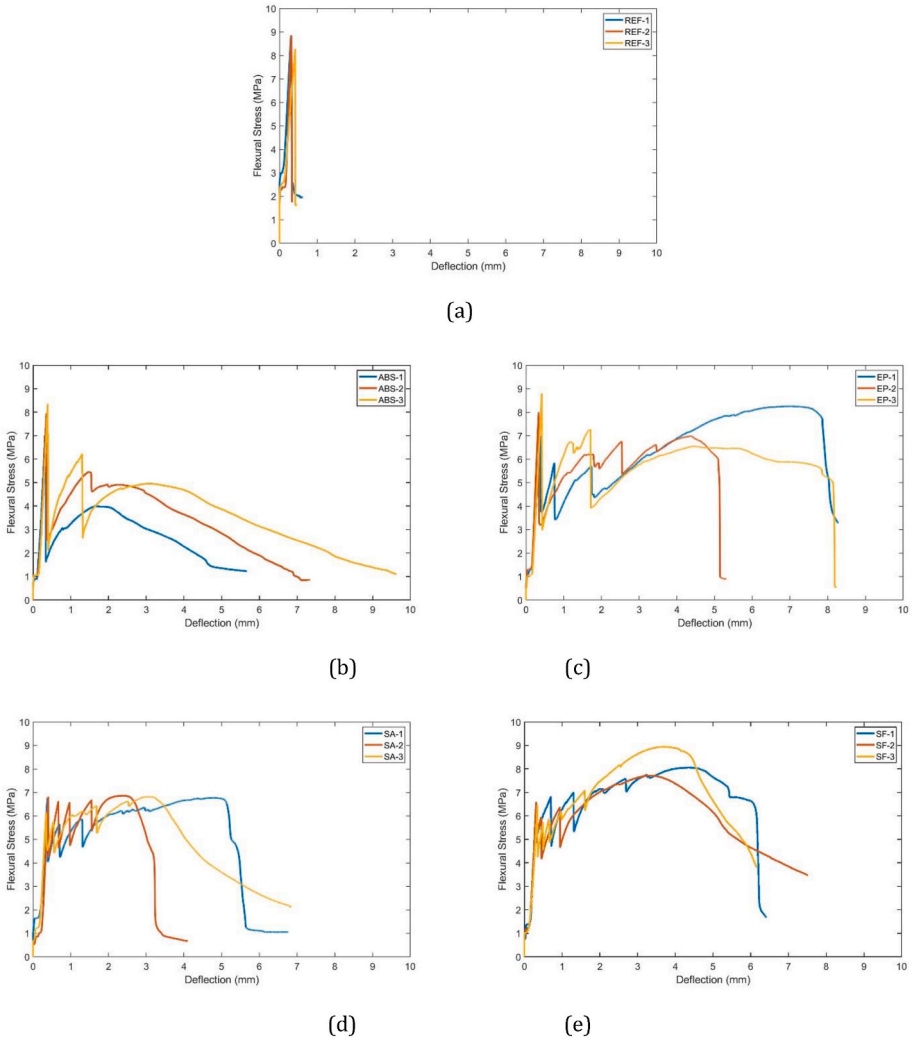

Fig. 12. Flexural-defection curves of a) reference mortar, b) ABS, c) epoxy, d) sand coated and e) steel fiber coated, results from three duplicates are indicated.

Fig. 13. Specimen with multiple cracks after four-point-bending test.

identified from the stress-displacement curves and shows similar slip behavior as the ABS. As a result, in the pull-out experiment the ABS and EP were pulled-out from the cementitious matrix. For the EP specimens, one test result shows that the reinforcement bar is ruptured inside the cementitious mortar (indicated by the sharp drop Fig. 11b EP-Exp), while the other three duplicates indicate that the reinforcement bar has been entirely pulled-out. This implies that the EP coating may already introduced improved bonding, but not significantly high enough to ensure the reinforcement not from being pulled-out from the cementitious mortar. Therefore, the pulled-out case of EP is regarded as experimental deviation not an outlier of the tests. And the pulled-out cases are taken as the general trend of the EP specimens.

This pull-out behavior of ABS and EP are successfully captured by the numerical simulations. It can be seen from Fig. 11a and b, the simulated stress-displacement curves agree well with the experiments: moderate post-peak softening is achieved, as a result of the slip between the reinforcement and the mortar. Correspondingly, the simulation results show that the ABS and EP reinforcement bar are pulled-out from the cementitious mortar as found in the experiment.

In sharp contrast, the sand coated (Fig. 11c, SA-Exp) and steel fiber coated (Fig. 11cd, SF-Exp) bars were ruptured in the experiment, instead of being pulled-out from the cementitious mortar. On the stress-displacement curves, this is identified by the steep stress drop after the peak load, as shown ind. In this sense, different from the ABS and EP reinforcement, the peak stress of SA and SF only indicates the strength of the reinforcement itself, not the bond strength between the reinforcement and mortar. The actual bond strength of the SA and SF would be even higher than the peak stress (approximately 3 MPa) as shown in Fig. 11c and d. This means that the sand coated (SA) and steel fiber coated (SF) reinforcement have considerably stronger bond with the cementitious mortar than the untreated ABS reinforcement (ABS) and

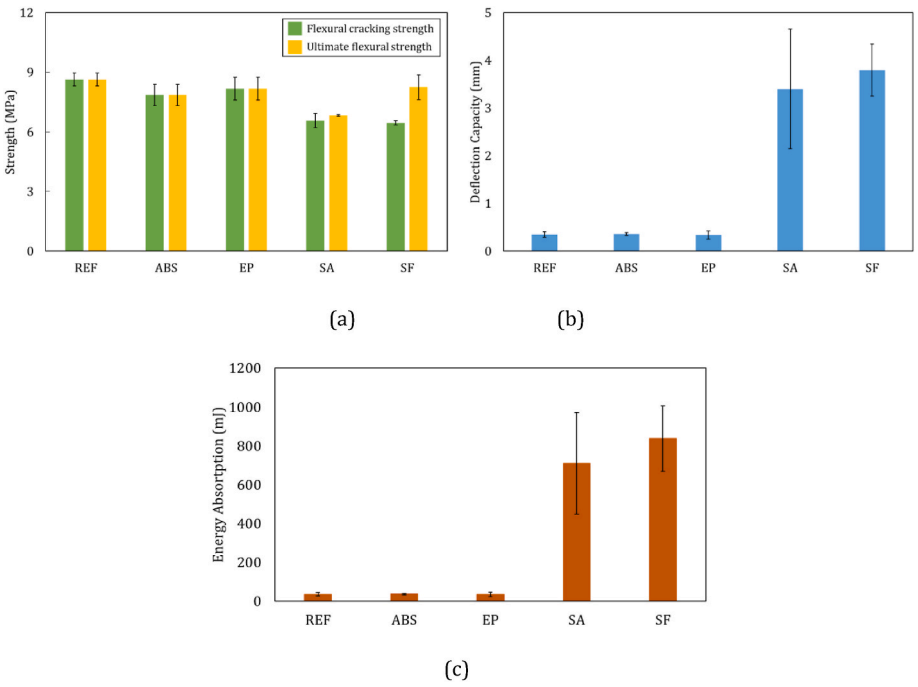

Fig. 14. a) Flexural cracking strength and ultimate strength; b) deflection capacity; c) energy absorption, standard deviation is indicated.

Table 5
Summary of flexural properties of all tested specimens, standard deviation is indicated.

Specimen	Flexural cracking strength (MPa)	Ultimate flexural strength (MPa)	Deflection capacity (mm)	Flexural energy absorption (mJ)
REF	8.63 ± 0.33	8.63 ± 0.33	0.35 ± 0.06	35.19 ± 8.00
ABS	7.85 ± 0.53	7.85 ± 0.53	0.36 ± 0.03	36.61 ± 3.94
EP	8.17 ± 0.57	8.17 ± 0.57	0.34 ± 0.08	35.85 ± 11.68
SA	6.57 ± 0.36	6.82 ± 0.05	3.40 ± 1.25	709.97 ± 261.64
SF	6.45 ± 0.11	8.24 ± 0.63	3.79 ± 0.55	837.50 ± 167.91

the reinforcement with only epoxy coating (EP). The modeling results show similar behavior: steep stress drop appears once peak stress is reached and both the SA and SF reinforcements are ruptured as seen in Fig. 11c and d.

As an inert material, the siliceous sand used in this work has no chemical bond with cementitious matrix. The improvement in the bond strength of the SA and SF is mostly attributed to the morphological effects. The rough surface of SA and SF reinforcement contributes to the significant improvement in the bond strength. Especially the steel fibers, they reached out from the reinforcement and formed numerous anchors tightly embedded in the cementitious mixture when casted in the cementitious mortar. Similar improvement effect by increasing the surface roughness of reinforcement was also observed on the sand coated textile reinforced concrete (Valeri et al., 2020b).

Note that in the lattice model of this work, the lattice element size within the entire lattice mesh needs to be the same. Therefore, the number of lattice elements will be enormous, if the morphology of the rough surface is geometrically represented as the sand and steel fibers are extremely small compared to the entire specimen. Limited by computing power, it was not possible to implement such representation in the present lattice model. Alternately, we increased the bonding strength and E-modulus of the SA-M and SF-M elements, to represent the improved bonding performance after surface treatment.

4.2. Flexural properties

The flexural stress-deflection curves of all tested specimens are shown in Fig. 12a. As expected, brittle fracture response is observed on the reference mortar REF the flexural stress immediately drops as soon as the peak stress (this peak stress is defined as the flexural cracking strength (Xu et al., 2019)) is reached, in the meanwhile, only one crack was observed on the specimens from the experiment. Similar behavior is also seen in other similar studies (Xu et al., 2019, 2021).

In sharp contrast, as shown from Fig. 12b to e, all the reinforced composites exhibit significantly more ductile fracture behavior: after the flexural cracking strength, the steep stress drop can be still found on all these curves, however, owing to the presence of the reinforcement the specimens did not fail immediately. Instead, the stress could increase again. As deflection increases, the widely known “multiple cracking” behavior (Li, 1993, 2003) was also observed during the experiment on the composites developed in this work (as seen in Fig. 13). Correspondingly, this is indicated by the multiple stress drops on the flexural-deflection curves as seen from Fig. 12b to e.

Among all reinforced specimens, the sand coated (SA, Fig. 12d) and steel fiber (SF, Fig. 12e) coated specimens show the highest ductility. Deflection-hardening behavior was achieved by the SA and SF, namely the stress increases to a higher value than the fracture strength. The highest flexural stress on the curves in is defined as the ultimate flexural strength (Xu et al., 2019). It can be seen from Fig. 14a, the ultimate flexural strength of SA and SF is higher than the flexural cracking strength. In comparison, the flexural cracking strength and ultimate flexural strength of ABS and EP specimens are identical.

The deflection-hardening behavior is a critical indicator of flexural ductility. Furthermore, the flexural ductility can be also quantified by the deflection capacity (define by the deflection at ultimate flexural strength). For all reinforced composites, the EP has obtained the highest flexural cracking strength of 8.16 MPa, which is 5.40% lower than the reference mortar REF, and 9.08 % higher than the unmodified ABS (7.85 MPa); The SF has an ultimate flexural strength of 8.24 MPa, which is 4.76 % slight lower than the EP and REF. The SA has obviously lower flexural strength of 6.82 MPa. Nevertheless, the SF and SA show significantly enhanced deflection-capacity (defined as the deflection at

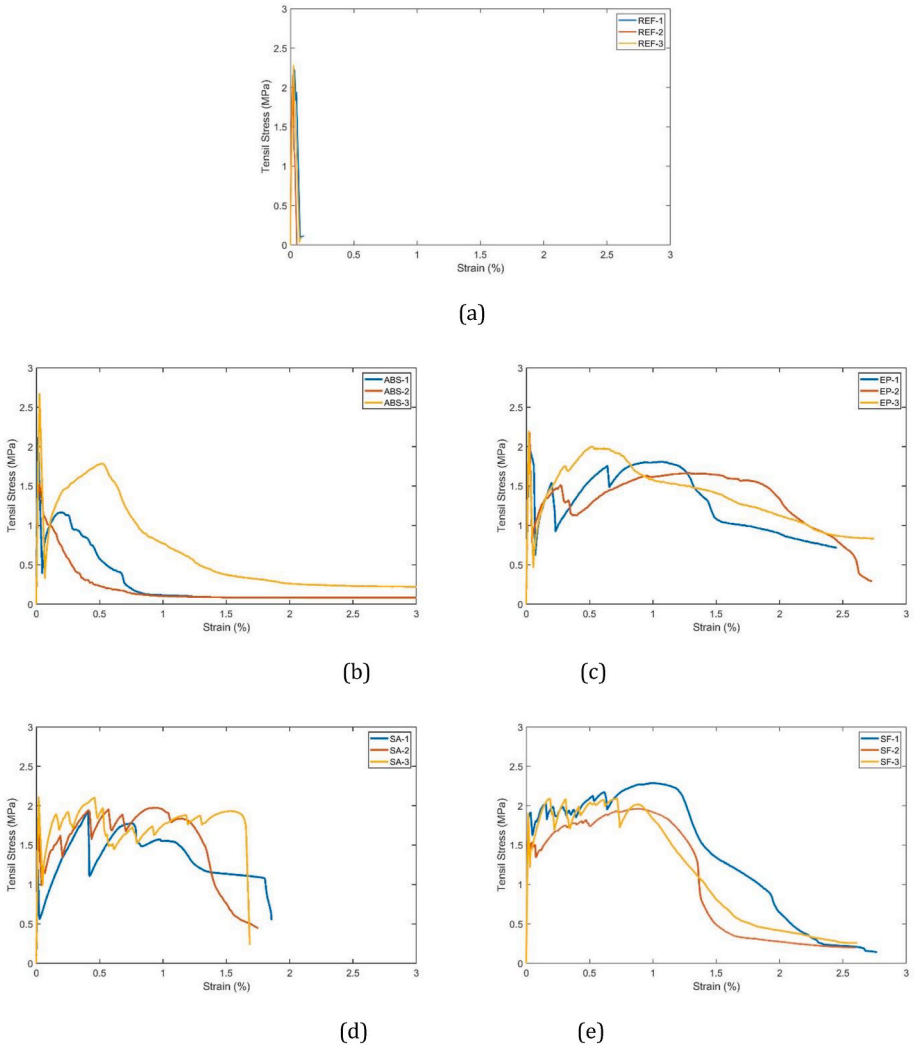

Fig. 15. Tensile stress-strain curves of the a) reference, b) ABS, c) epoxy, d) sand coated and e) steel fiber coated.

maximum stress) as shown in Fig. 14b. Specifically, the SF shows the highest deflection capacity of 3.79 mm, which is more than 10 times higher than the REF and ABS. A summary of the flexural properties of all tested specimens is listed in Table 5. The increase in deflection capacity significantly enhanced the flexural energy absorption (defined by the area below load-deflection curves up to the deflection capacity) of the composites. As can be seen in Fig. 14c, the flexural energy absorption of the SA and SF specimens is much higher than all other specimens. It's well known that the flexural ductility of reinforced cementitious composites is highly dependent on the bonding properties between the reinforcement and cementitious mortar. Similar behaviors can be also found in this work. According to Fig. 11, the SA and SF shows significantly higher bonding strength than the ABS and EP specimens. As a results, the SA and SF achieved significantly higher flexural ductility. Moreover, the bonding strength of SF is also slightly higher that the SA which also ensured the SF with better ductility than the SA. More detail analysis on the role of the bonding behavior will be given in section 4.4.

In summary, the surface-modified reinforcement ensures the composites with improved flexural properties comparing to the unmodified ABS. Specifically, the steel fiber coated reinforcement performs the best, considering the slightly lower ultimate flexural strength but strikingly higher deflection capacity. Compared to our previous study, the SF achieved similar deflection capacity to the composite reported in (Xu et al., 2019) which had almost 2 times higher reinforcing ratio.

4.3. Tensile properties

Due to their intrinsic brittleness, cementitious materials are prone to cracking under tensile load. Therefore, the flexural behavior of cementitious composites is normally dictated by the tensile behavior. In this sense, the tensile behavior gives more direct indication on the impact of surface coating techniques on improving the mechanical performance of the composites. It can be seen from Fig. 15a, the REF specimens exhibit expected brittle tensile fracture behavior, indicated by the immediate stress drop after the tensile cracking strength (defined as the stress of the first peak on the stress-strain curve). In contrast, all reinforced composites show considerably more ductility under tensile load as expected, as seen by the stress increase after the tensile cracking strength on the stress-strain curves shown from Fig. 15c–e.

In addition, the EP, SA and SF achieved multiple cracking under tension load (crack pattern shown in Fig. 18), while only the SA and SF achieved the target strain-hardening behavior. This can be seen from Fig. 15c–e, multiple stress drops are witnessed after the tensile cracking strength is reached. In comparison, for ABS (Fig. 15a), only one main stress drop is seen, even though the stress could increase after the tensile cracking strength. Furthermore, only the SA and SF obtained the so-called strain-hardening behavior. This means that the ultimate tensile strength (defined as the highest stress on the curves) is higher than the cracking strength, as shown in Fig. 16a. Moreover, the strain value at the ultimate tensile strength is defined as the strain capacity of the

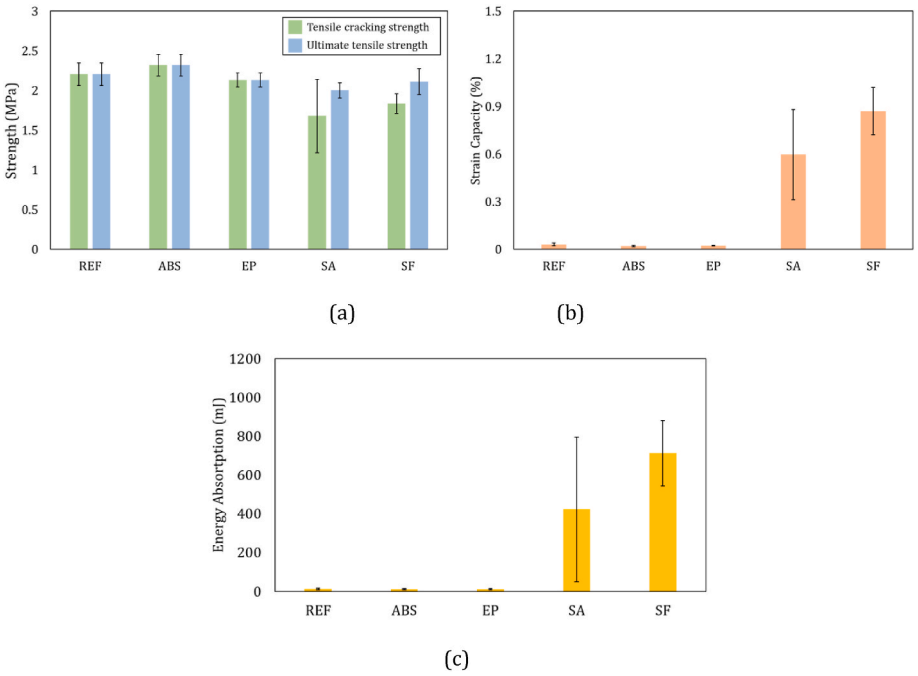

Fig. 16. a) Tensile strength and b) strain capacity and c) energy absorption of all tested specimens, standard deviation is indicated.

Table 6
Summary of tensile properties of all tested specimens, standard deviation is indicated.

Specimen	Tensile cracking strength (MPa)	Ultimate Tensile strength (MPa)	Strain capacity (%)	Energy absorption (mJ)
REF	2.21 ± 0.14	2.21 ± 0.14	0.03 ± 0.01	13.08 ± 4.23
ABS	2.32 ± 0.14	2.32 ± 0.14	0.02 ± 0.01	11.35 ± 3.34
EP	2.13 ± 0.09	2.13 ± 0.09	0.02 ± 0.01	11.22 ± 3.17
SA	1.68 ± 0.46	2.00 ± 0.10	0.60 ± 0.28	422.73 ± 372.51
SF	1.83 ± 0.13	2.11 ± 0.16	0.87 ± 0.15	711.55 ± 168.67

composites. It is clearly seen in Fig. 16b, that the strain capacity of the SA and SF is strikingly higher than the ABS. Especially, the strain capacity of the SF reached 0.9%. This is approximately 30% higher than the composite in (Xu et al., 2019) which is reinforced with the same 3D printed material but two times higher reinforcing ratio than the SF specimens in this work. Similar to the behavior in bending, the increase in tensile strain capacity significantly improved the energy absorption (defined as the area below load-displacement curves up to the strain capacity) of the cementitious composites. As can be seen in Fig. 16c, the energy absorption of SA and SF is strikingly higher than the other specimens. These results reveal that using sand and steel fiber as surface modification significantly improved the ductility of composites with 3D printed polymeric reinforcement. A summary of the tensile properties from all tested specimens is listed in Table 6.

4.4. Impact of interface on the composite behavior

The experimental results clearly indicate that the surface treated reinforcement (especially by sand and steel fibers) significantly improved the flexural and tensile properties of the composites. In this section, the critical role of the surface treatment on influencing the bonding properties, and the subsequent impact on determining the composites' mechanical properties will be analyzed.

The pull-out tests particularly revealed the impact of the surface treatment on the bond strength. In addition, the mechanical properties of the composites were also crucially dictated by the bond strength. Fig. 17 shows the comparison between simulation and experimental results of the uniaxial tensile behavior of the composites. In general, the simulation results highly agree with the experiments. Especially the post-peak behavior: the simulation successfully captured the stress increase after the first peak, and the multiple cracking as indicated by multiple stress drops after the first peak. It can be also seen from the experimental DIC results and the numerical simulated crack pattern (Fig. 18) that the EP, SA and SF exhibit multiple cracks while the ABS only shows one crack. More importantly, as seen in Fig. 17, the simulation results also suggests that only the SA (Fig. 17c) and SF (Fig. 17d) composites exhibit the strain-hardening behavior, which is highly consistent with the experimental results. Still, it is worth mentioning that the first stress drop of the simulated curves looks more significant than the experiments. This is mainly caused by the pure brittle (namely, one segment as can be seen in Table 4) input of the mortar element. In the uniaxial tensile tests of the unreinforced mortar, no post-peak behavior (Fig. 15a) was recorded due to the rapid cracking of cementitious mortar. Therefore, in the lattice model, it was not possible to calibrate the post-peak softening part of the mortar elements. So, only pure brittle cracking behavior (one segment) was be assigned to these elements. As a result, the simulated first crack seems more significant than the experimental results. In case the post-peak cracking behavior of the cementitious mortar can be properly captured by experiments, multiple segments may be also assigned to the mortar elements and this difference will be mitigated.

In the numerical simulations, the difference in the bonding input properties (ABS-M, EP-M, SA-M and SF-M in Table 4) is outstanding compared to other input values. As listed in Table 4, after coating epoxy, the bonding strength of EP-M (2.5 MPa) was not significantly improved compared to ABS-M (2.2 MPa), and the simulated stress-strain curve of ABS and EP resembles each other (see Fig. 17a–b): after the cracking strength the stress could increase again but couldn't reach values higher than the first cracking strength. Because the EP reinforcement shows somewhat higher strength (42 MPa) than the ABS reinforcement (35 MPa), the stress-strain curves of EP also indicate slight better ductility than ABS. This is seen by the longer softening branch of the EP as seen in Fig. 17. In sharp contrast, as already discussed before, the sand coated

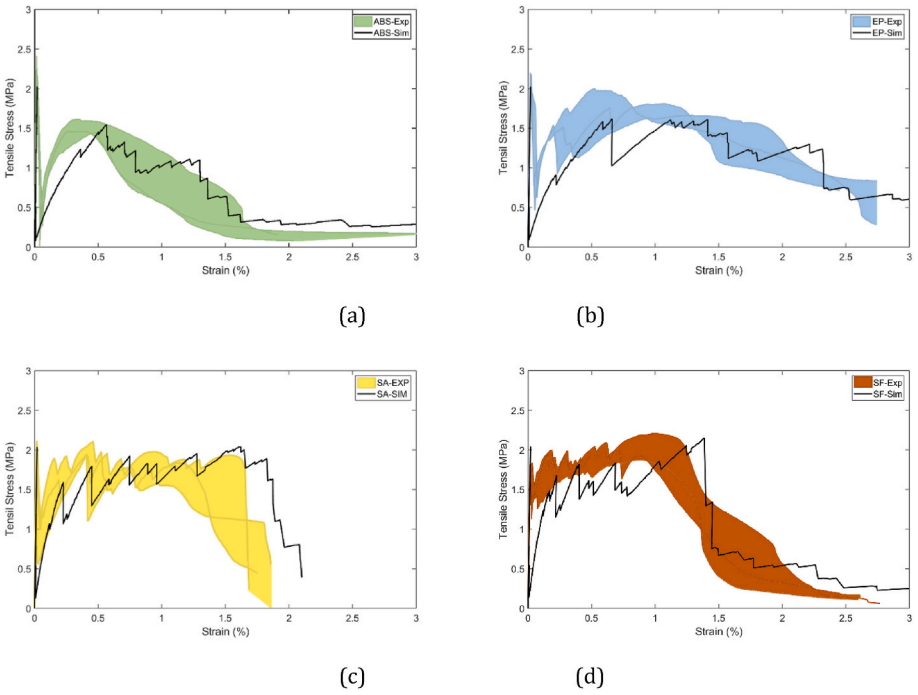

Fig. 17. Comparison between simulated and experimentally obtained stress-strain curves of the composites reinforced with a) ABS, b) EP, c) SA and d) SF.

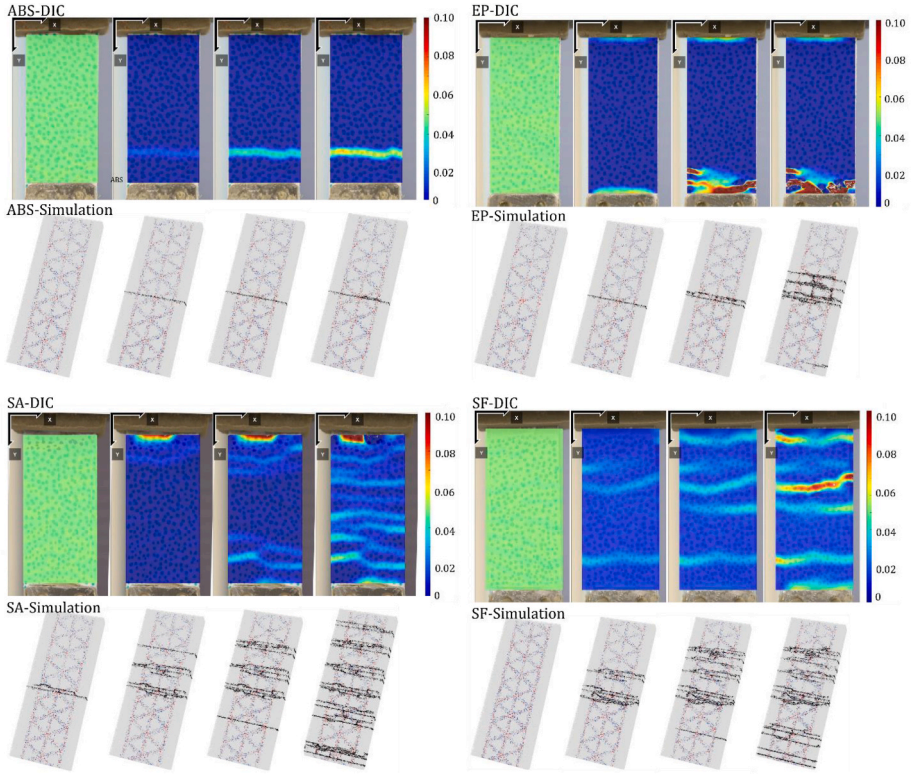

Fig. 18. Crack pattern obtained from experiment (DIC) and simulation, strain scale is indicated in the DIC figures, failed elements (cracks) are indicated in black of the simulation results.

(SA) and steel fiber coated (SF) reinforcement achieved improved the interface bonding strength. Correspondingly, the model input bonding strength of SF-M and SA-M were also increased to 35 MPa and 45 MPa to properly simulate this significantly improvement. These two values are already 1590% and 2045 % higher than ABS-M, meanwhile 1400% and 1800% higher than EP-M. It's worth mentioning that, in Table 4 the input E-modulus of SA-M and SF-M is also higher than the ABS-M and EP-M. This is also a result of the improved bonding between the reinforcement and the cementitious matrix. As no pulled-out was observed, the mean E-modulus value of the reinforcement (SA and SF) and cementitious mortar is used as the interface element (SA-M and SF-M) E-modulus. The simulated SA and SF composites can successfully capture

the improved tensile performance of the SA and SF. As seen in Fig. 17c–d, both SA-Sim and SF-Sim achieved the strain-hardening behavior and the multiple cracking behavior (indicated by multiple steep stress drops) observed in the experiment.

In the numerical model, the physical meaning of the model elements is only differentiated by the input values. Therefore, it is not difficult to isolate the role of different elements by varying the input values and compare the consequences. In the present work, only when the strength of the interface element was significantly increased approximately 14–20 times, the simulated tensile behavior of the cementitious composites can properly capture the experimental findings. Similar trend of the influence of the bonding properties can be also found on the flexural behavior of the composites as already mentioned in section 4.2. These results strongly indicate that the interface bonding strength is a determinative factor on dictating the ductility of cementitious composites reinforced by 3D printed polymeric structures, and improving the bonding strength would significantly improve the ductility of the reinforced composites.

5. Conclusions

This work presents a study on using surface treatment to improve the mechanical performance of cementitious composites reinforced with 3D printed lattice structures. Three types of surface coatings were used: epoxy resin (EP), sand sprinkled epoxy (SA) and short steel fibers sprinkled epoxy (SF). Experiments and numerical simulations were performed to evaluate the reinforcement-mortar bonding properties, and the mechanical properties of the reinforced cementitious composites. According to the obtained results, several conclusions can be drawn:

- The SA and SF surface coatings can significantly improve the bonding strength between 3D printed ABS reinforcement and cementitious mortar. The uncoated ABS reinforcement (1.5 MPa) and EP coated reinforcement (2 MPa) both exhibit low bonding strength with cementitious mortar. After coated with sand and steel fiber, the bonding strength increases to more than 3 MPa.
- All specimens with surface coated reinforcement exhibit enhanced mechanical performance than the cementitious composites with uncoated reinforcement. Especially, the SA and SF show outstandingly better performance. The deflection capacity of cementitious composites reinforced by SA and SF reinforcement is approximately 10 times of the specimens with uncoated reinforcement, and the specimens coated with EP reinforcement. Only the specimens with SA and SF reinforcement achieved tensile strain-hardening behavior. Comparted to the specimens with uncoated reinforcement and EP reinforcement, the strain capacity of the SA and SF specimens is increased by 3000% and 4350%, respectively.
- The numerical simulation results agree well with the experimental findings, and confirmed that the interface bonding strength is the critical factor of determining the ductility of cementitious composites reinforced with 3D printed polymers. Although in the numerical model all three types of coatings slightly increased the strength of the reinforcement elements, only when the strength of interface elements is significantly increased (which is the case of SA and SF) the reinforced cementitious composites can properly capture the improved ductility as found in the experiments.

CRediT authorship contribution statement

Yading Xu: Writing – review & editing, Writing – original draft, Investigation, Formal analysis, Conceptualization. **Zhi Wan:** Writing – review & editing, Investigation, Formal analysis, Conceptualization. **Branko Šavija:** Writing – review & editing, Resources, Project administration, Methodology, Funding acquisition.

Declaration of competing interest

The authors declare no conflict of interest.

Data availability

Data will be made available on request.

Acknowledgements

Yading Xu and Branko Šavija acknowledge the financial support from the European Research Council (ERC) within the framework of the ERC Starting Grant Project “Auxetic Cementitious Composites by 3D printing (ACC-3D)”, Grant Agreement Number 101041342. Views and opinions expressed are however those of the author(s) only and do not necessarily reflect those of the European Union or the European Research Council. Neither the European Union nor the granting authority can be held responsible for them.

References

Abbas, M., Bary, B., Jason, L., 2023. 3D mesoscale analysis of the effects of steel bar ribs geometry on reinforced concrete bond strength. Finite Elem. Anal. Des. 219, 103928.
Alatawna, A., et al., 2021. Textile-cement bond enhancement: sprinkle some hydrophilic powder. Cement Concr. Compos. 120, 104031.
Chaves Figueiredo, S., et al., 2019. An approach to develop printable strain hardening cementitious composites. Mater. Des. 169, 107651.
Chen, M., et al., 2023. Geometric design and performance of single and dual-printed lattice-reinforced cementitious composite. Cement Concr. Compos. 143, 105266.
Cho, K., et al., 2006. Bond-slip model for coarse sand coated interface between FRP and concrete from optimization technique. Comput. Struct. 84 (7), 439–449.
Dey, D., et al., 2023. Flexural performance of 3D printed concrete structure with lattice infills. Develop. Built Environ. 16, 100297.
Ertzibengoa, D., Matthys, S., Taerwe, L., 2012. Bond behaviour of flat stainless steel rebars in concrete. Mater. Struct. 45 (11), 1639–1653.
Farina, I., et al., 2016. On the reinforcement of cement mortars through 3D printed polymeric and metallic fibers. Compos. B Eng. 90, 76–85.
Halvaei, M., Latifi, M., Jamshidi, M., 2018. Study of the microstructure and flexural behavior of cementitious composites reinforced by surface modified carbon textiles. Construct. Build. Mater. 158, 243–256.
Lao, J.-C., et al., 2024. Fly ash-dominated high-strength engineered/strain-hardening geopolymer composites (HS-EGC/SHGC): influence of alkalinity and environmental assessment. J. Clean. Prod. 447, 141182.
Li, V.C., 1993. From Micromechanics to Structural Engineering-The Design of Cementitous Composites for Civil Engineering Applications.
Li, V.C., 2003. On Engineered Cementitious Composites (ECC).
Li, Z., Wang, L., Ma, G., 2020a. Mechanical improvement of continuous steel microcable reinforced geopolymer composites for 3D printing subjected to different loading conditions. Compos. B Eng. 187, 107796.
Li, V.C., et al., 2020b. On the emergence of 3D printable engineered, strain hardening cementitious composites (ECC/SHCC). Cement Concr. Res. 132, 106038.
Li, Q.-H., et al., 2024. Bond behavior between steel bar and strain-hardening fiber-reinforced cementitious composites under fatigue loading. Eng. Struct. 314, 118354.
Lim, J.H., Panda, B., Pham, Q.-C., 2018. Improving flexural characteristics of 3D printed geopolymer composites with in-process steel cable reinforcement. Construct. Build. Mater. 178, 32–41.
Liu, J., et al., 2023. 3D printing of cementitious mortar with milled recycled carbon fibres: influences of filament offset on mechanical properties. Cement Concr. Compos. 142, 105169.
Lu, J., et al., 2021. Bond performance of sand-coated and ribbed-surface glass fiber reinforced polymer bars in high-performance concrete. Structures 34, 10–19.
Mechtcherine, V., et al., 2018. 3D-printed steel reinforcement for digital concrete construction – manufacture, mechanical properties and bond behaviour. Construct. Build. Mater. 179, 125–137.
Nguyen-Van, V., et al., 2022a. Dynamic responses of bioinspired plastic-reinforced cementitious beams. Cement Concr. Compos. 133, 104682.
Nguyen-Van, V., et al., 2022b. Performance of concrete beam reinforced with 3D printed Bioinspired primitive scaffold subjected to three-point bending. Autom. ConStruct. 134, 104060.
Preinstorfer, P., et al., 2023. Cracking behaviour of textile-reinforced concrete with varying concrete cover and textile surface finish. Compos. Struct. 312, 116859.
Rabi, M., et al., 2020. Bond behaviour of austenitic stainless steel reinforced concrete. Eng. Struct. 221, 111027.
Rafique, N., et al., 2020. Feasibility of textile fabrics for strengthening of concrete column. Construct. Build. Mater. 259, 119684.
Redon, C., et al., 2001. Measuring and modifying interface properties of PVA fibers in ECC matrix. J. Mater. Civ. Eng. 13 (6).
Reis, E.D., et al., 2023. Bonding of steel bars in concrete: a systematic review of the literature. Structures 49, 508–519.

Salazar, B., et al., 2020. Polymer lattice-reinforcement for enhancing ductility of concrete. Mater. Des. 196, 109184.
Schlangen, E., Garboczi, E.J., 1997. Fracture simulations of concrete using lattice modles: computational aspects. Eng. Fract. Mech. 57, 319–332.
Sigrüner, M., Hüsken, G., Pirskawetz, S., Herz, J., Muscat, D., Strübbe, N., 2023. Pull-out behavior of polymer fibers in concrete. J. Polym. Sci. 61 (21), 2708–2720.
Skoratko, A., et al., 2022. Mechanical properties of mortar beams reinforced by gyroid 3D printed plastic spatial elements. Cement Concr. Compos. 134, 104809.
Tang, C., et al., 2023. Flexural properties of 3D printed graded lattice reinforced cementitious composites using digital image correlation. Mater. Des. 227, 111734.
Valeri, P., Ruiz, M.F., Muttoni, A., 2020a. Modelling of textile reinforced concrete in bending and shear with elastic-cracked stress fields. Eng. Struct. 215, 110664.
Valeri, P., Fernàndez Ruiz, M., Muttoni, A., 2020b. Tensile response of textile reinforced concrete. Construct. Build. Mater. 258, 119517.
Wu, H., et al., 2023. Interfacial bond properties and pullout behaviors of steel fibers embedded in ultra-high-performance concrete: a review. Mater. Today Commun. 35, 106081.
Xu, Y., Šavija, B., 2019. Development of strain hardening cementitious composite (SHCC) reinforced with 3D printed polymeric reinforcement: mechanical properties. Compos. B Eng. 174, 107011.
Xu, Y., et al., 2021. Cementitious composites reinforced with 3D printed functionally graded polymeric lattice structures: experiments and modelling. Addit. Manuf., 101887
Xu, Y., et al., 2022. Towards understanding deformation and fracture in cementitious lattice materials: insights from multiscale experiments and simulations. Construct. Build. Mater. 345.
Xu, Y., Šavija, B., 2024a. Auxetic cementitious composites (ACCs) with excellent compressive ductility: experiments and modeling. Mater. Des. 237.
Xu, Y., et al., 2024b. Spring-like behavior of cementitious composite enabled by auxetic hyperelastic frame. Int. J. Mech. Sci. 275, 109364.
Zhou, Y., et al., 2021. Enhancing the PVA fiber-matrix interface properties in ultra high performance concrete: an experimental and molecular dynamics study. Construct. Build. Mater. 285, 122862.
Zhu, J.-X., et al., 2024. Ultra-High-Strength Engineered Cementitious Composites (UHS-ECC) panel reinforced with FRP bar/grid: development and flexural performance. Eng. Struct. 302, 117193.